Electronic Supplementary Material (ESI) for Journal of Materials Chemistry A.

Electronic Supplementary Information to

Solution-based ALD route towards $(CH_3NH_3)(PbI_3)$ perovskite *via* lead sulfide films

Vanessa M. Koch,[a] Maïssa K. S. Barr,[a] Pascal Büttner,[a] Ignacio Mínguez-Bacho,[a] Dirk Döhler,[a] Bettina Winzer,[b] Elisabeth Reinhardt[bc] Doris Segets,[d] and Julien Bachmann* [ae]

[a] Department of Chemistry and Pharmacy, Chemistry of Thin Film Materials, Friedrich-Alexander-Universität Erlangen-Nürnberg, IZNF Cauerstr. 3, 91058 Erlangen, Germany

[b] Institute of Particle Technology (LFG), Friedrich-Alexander-Universität Erlangen-Nürnberg, Cauerstraße 4, 91058 Erlangen, Germany

[c] Interdisciplinary Center for Functional Particle Systems (FPS), Friedrich-Alexander-Universität Erlangen-Nürnberg, Haberstraße 9a, 91058 Erlangen, Germany

[d] Process Technology for Electrochemical Functional Materials, Institute for Combustion and Gas Dynamics – Reactive Fluids (IVG-RF) and Center for Nanointegration Duisburg-Essen (CENIDE, University of Duisburg-Essen (UDE), Carl-Benz-Straße 199, 47057 Duisburg. Germany

[e] Institute of Chemistry, Saint Petersburg State University, Universitetskii pr. 26, Saint Petersburg 198504, Russian Federation

Experimental details

All chemicals mentioned in the following were used without any further purification.

Instrumental Methods. Spectroscopic ellipsometry measurements were performed using a SENPro spectroscopic ellipsometer from SENTECH. All measurements were conducted under an angle of 70 ° in a spectral range of 370 – 1050 nm. Data analysis was performed with the software SpectraRay 4. X-ray reflectometry (XRR) and atomic force microscopy (AFM) were used to verify the thicknesses obtained by spectroscopic ellipsometry and to determine the roughness. For XRR, a D8 DISCOVER X-ray diffractometer from Bruker with a Cu Kα source (20 kV) was used. Data analysis was performed *via* the corresponding software DIFFRAC.LEPTOS. AFM measurements in tapping mode with a MultiMode SPM NanoScope 3 atomic force microscope from Digital Instruments were performed (Institute of Particle Technology (LFG), Friedrich-Alexander University Erlangen-Nürnberg, Germany) and a Dimension V AFM from Veeco. Scanning electron microscopy (SEM) was conducted using a JEOL JSM-6400 scanning electron microscope with an integrated SDD detector to measure EDX. The acceleration voltage was 20 kV and as cathode material, LaB_6 was used. In addition, a GeminiSEM 500 thermal field-emission SEM from Zeiss with an acceleration voltage of 5 kV was used for high-resolution SEM micrographs. X-ray diffraction in grazing incidence (GI-XRD) using a D8 DISCOVER X-ray diffractometer from Bruker with a Cu Kα source (20 kV) was performed to determine the crystallinity of the samples. X-ray photoelectron spectroscopy (XPS) measurements were performed with a PHI Quantera SXM X-ray photoelectron spectrometer from Physical Electronics Inc. with an Al Kα source. Fitting of the XPS spectra was performed with the software CasaXPS, version 2.3. All XPS spectra were charge-referenced to adventitious carbon (C 1s) at a binding energy (BE) of 284.8 eV. Temperature-dependent Hall measurements using a Variable Temperature Hall System from MMR Technologies with a H5000 VTHS Controller and a K2000 Digital Temperature Controller in the range from 120 K – 380 K with a magnetic field of +/− 3600 G were carried out (square geometry of the sample).

Preparation of the substrates. Silicon (100) wafers with 200 nm thermal oxide were purchased from Silicon Materials Inc. Si/SiO_2 wafers gALD-coated with anatase TiO_2 were used for the optimization of the PbS sALD parameters. TiO_2 served as reference for the PbS deposition since it is a widely used Electron Transporting Material (ETM) in photovoltaic devices.[1] Hence, TiO_2 films were deposited *via* gALD on Si/SiO_2 wafers using a GEMStar-6 XT ALD reactor from Arradiance. For the TiO_2 gALD, titanium(IV) isopropoxide (TTIP, purchased from Alfa Aesar) and distilled H_2O were used as precursors. TTIP was kept at 70 °C whereas H_2O was kept at

room temperature. The temperature of the reaction chamber was set to 120 °C. The pulse durations for TTIP and H_2O were 1 s and 0.2 s, respectively. The exposure duration for each precursor was 15 s. Each precursor pulse was followed by a 40-s purge with N_2.[2] Since TiO_2 gALD at low temperatures results in the deposition of amorphous TiO_2,[3,4] subsequent annealing in a muffle furnace at 450 °C for 4 h, with a ramp of 4 h from room temperature to 450 °C, in N_2 atmosphere was carried out to obtain the anatase phase of TiO_2. To investigate the effect of a S-terminated surface on the PbS growth, amorphous ZnS[5] was deposited *via* gALD with the aforementioned ALD reactor on Si/SiO_2 wafers. Diethylzinc (purchased from Merck KGaA) and hydrogen sulfide (H_2S, 2.995 Vol % in N_2, purchased from Air Liquide S.A) were used as precursors. Both precursors were kept at room temperature. The temperature of the reaction chamber was set to 120 °C. The pulse and purge durations for both precursors were 0.2 s and 15 s, respectively. The exposure duration for each precursor was set to 15 s.[5,6] Aluminum platelets (99.99%) from SmartMembranes were used for preparing AAO membranes with a length of approximately 5 µm. The AAO membranes were prepared according to a standard two-step anodization procedure using phosphoric acid.[7]

sALD setup and deposition of PbS. PbS sALD was carried out in a home-built microfluidic setup with peristaltic OEM pumps described earlier by Y. Wu *et al*.[8] and J. Fichtner *et al*.[9] The sALD setup and the corresponding software were constructed by ZUMOLab GbR. The OEM peristaltic pumps (model 400A, 0 – 24 V) as well as the fittings, the Luer-lock connectors and the fluoroelastomeric flexible tubes were purchased from Watson-Marlow. Lead(II) nitrate ($Pb(NO_3)_2$, purchased from Merck Millipore) and sodium sulfide nonahydrate ($Na_2S \cdot 9H_2O$, purchased from Alfa Aesar) were used as the two precursors for sALD of PbS. MeOH (purchased from Thermo Fisher Scientific Inc.) was used to dissolve $Pb(NO_3)_2$ and $Na_2S \cdot 9H_2O$, respectively. MeOH was used as the purging solvent as well. Fresh solutions of $Pb(NO_3)_2$ and $Na_2S \cdot 9H_2O$ dissolved in MeOH, respectively, were prepared under inert conditions. Both precursor solutions were ultrasonicated for 10 min before use. The standard experimental parameters for PbS sALD are as follows: 1 mM concentration for $Pb(NO_3)_2$ and $Na_2S \cdot 9H_2O$, respectively. 15 s pulse duration and 40 s purge duration for both precursors. The ratio of both precursors was kept constant at 1 : 1. The pulse and purge durations were varied to investigate the saturation behavior, *i.e.* the pulse duration was varied while the purge duration was kept constant and *vice versa* (see Results and discussion). During sALD, N_2 was gently bubbled through the precursor solutions with stainless-steel cannulae connected to a Schlenk line. The cannulae and the flexible PTFE tubes were purchased from VWR. The microscope glass slide (made of soda lime glass, purchased from Carl Roth GmbH & Co. KG.) which sealed the chamber under the pressure exerted by a thick acrylic glass piece also served as a substrate. The glass slide was cleaned with detergent in distilled water, isopropanol and acetone and dried in N_2 flow. The planar substrates were placed in the PTFE chamber whereas the AAOs were taped with Kapton® tape inside the chamber. The substrates were exposed to the precursor solutions flowing by their surface in an alternating manner with a purge step after each precursor

pulse. The power of all four pumps was set to 100%, which is equivalent to a flow rate of approximately 0.69 mL/min. After the deposition was finished, the samples were removed from the chamber, rinsed with MeOH and dried in N_2 flow. The annealing experiments were performed under N_2 atmosphere in a tube furnace. The temperature was ramped up from room temperature to 300 °C over 4 h, maintained at 300 °C for 4 h, then the furnace was turned off to cool the samples to room temperature under N_2.

Conversion of PbS to MAPI. The PbS synthesized was converted to MAPI based on a method described by H. A. Abbas *et al*.[10] They converted PbI_2 to MAPI by exposing the solid to vapors of methylammonium iodide. Hence, we transferred this principle to PbS. The PbS-coated substrates were placed on a hotplate in N_2 atmosphere, homogeneously surrounded by ground methylammonium iodide (MAI, synthesized based on a literature procedure,[11] and recrystallized from ethanol) and covered by a watch glass. The substrates were heated at 150 °C until the conversion of PbS to MAPI, indicated by a visible color change, was completed. After conversion, the hotplate was cooled down to 100 °C. Upon reaching 120 °C, the watch glass was removed. The substrates were kept at 100 °C for 10 min to avoid too fast crystallization. The samples were stored under N_2 atmosphere at room temperature after complete conversion. For a successful conversion of PbS to MAPI, the MAI powder needs to be placed in close vicinity to the PbS substrates and the MAI vapors forming upon subliming the MAI should be homogeneously distributed inside the chamber to allow for a homogeneous conversion.

Additional figures

Solution ALD of PbS

The precipitation of PbS from $Pb(NO_3)_2$ and $Na_2S \cdot 9H_2O$ facilitates a homogeneous deposit and a color change on TiO_2-coated and ZnS-coated Si/SiO_2 wafers, respectively, and results in a brown, homogeneous deposit on the microscope glass slide. Corresponding photographs are shown in **Figure S1**.

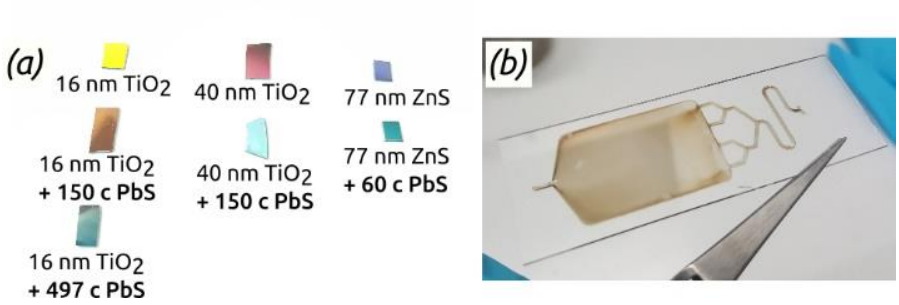

Figure S1 – (a) Photograph of uncoated and with PbS coated TiO_2 and ZnS substrates. Cycles is abbreviated with 'c'. The photograph was overexposed to make the color change more visible. (b) Photograph of the microscope glass slide used to cover the microfluidic chamber coated with 197 cycles of PbS sALD. The design of the microfluidic chamber is resembled in the PbS deposition.

PbS material characterization

AFM micrographs of PbS (60 and 497 sALD cycles, respectively) deposited on TiO_2 are presented in **Figure S2**. Uncoated TiO_2 is used as reference. The roughness *RMS* is a) *RMS* 0.4 nm, b) *RMS* 6.0 nm and c) *RMS* 40.9 nm.

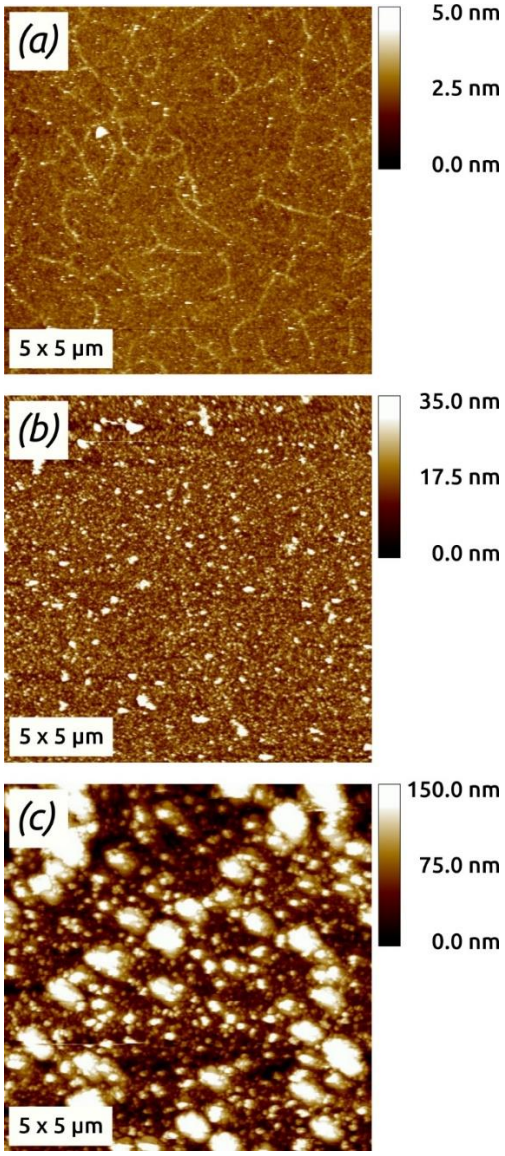

Figure S2 – AFM micrographs of (a) bare TiO_2, (b) 60 cycles PbS and (c) 497 cycles PbS on TiO_2.

AFM micrographs of PbS (150, 250 and 400 sALD cycles) deposited on ZnS are depicted in **Figure S3**. Uncoated ZnS is used as reference. The roughness *RMS* of the samples is a) *RMS* 1.3 nm, b) *RMS* 14.3 nm, c) *RMS* 23.5 nm and d) *RMS* 28.8 nm.

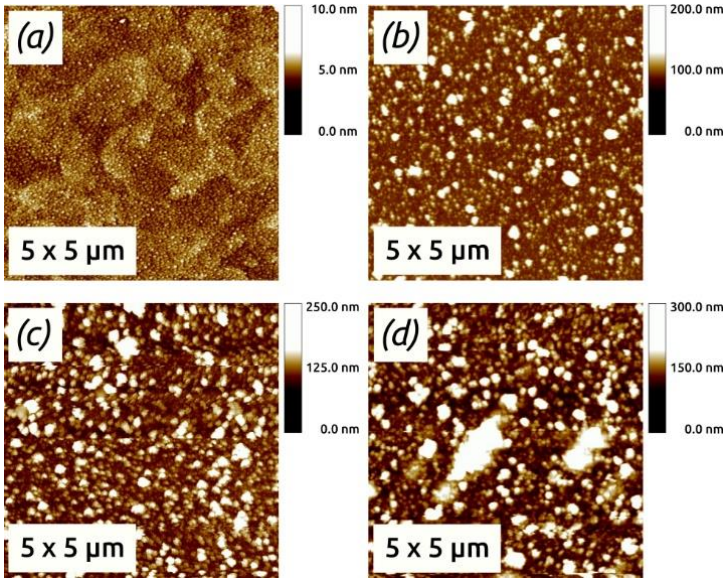

Figure S3 – AFM micrographs of (a) bare ZnS, (b) 150 cycles PbS, (c) 250 cycles PbS and (c) 400 cycles PbS on ZnS.

The EDX results of PbS (497 sALD cycles) deposited on TiO_2 are shown in **Figure S4**. The main contribution is Si at 1.74 eV ($K\alpha_1$) with 59.55 *at%* from the Si wafer. O at 0.52 eV ($K\alpha_1$) with 22.92 *at%* can be related to SiO_2 and TiO_2. The signal at 0.26 eV ($K\alpha_1$) for C with 16.19 *at%* result from atmospheric carbon and the sample holder. The signal at 4.49 eV ($K\alpha_1$) for Ti exhibits a low amount of 0.20 *at%*, which indicates full coverage of the TiO_2 surface with PbS. The signal for S appears at 2.31 eV ($K_{\alpha 1}$) with 0.66 *at%*. Signals for Pb appear at 2.34 eV ($M\alpha_1$), 10.54 eV ($L\alpha_1$) and 12.62 eV ($L\alpha_1$).[12]

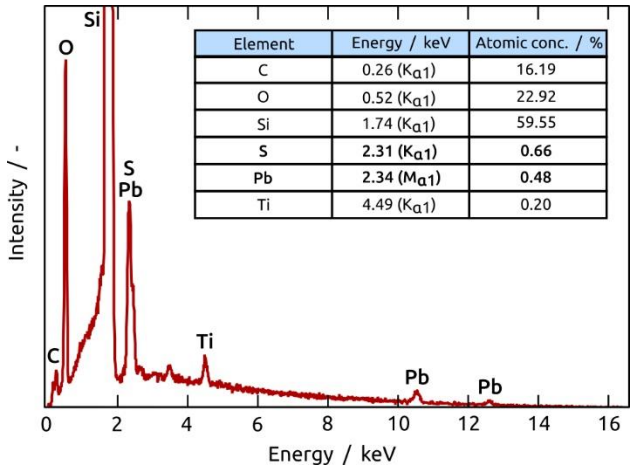

Element	Energy / keV	Atomic conc. / %
C	0.26 ($K_{\alpha 1}$)	16.19
O	0.52 ($K_{\alpha 1}$)	22.92
Si	1.74 ($K_{\alpha 1}$)	59.55
S	**2.31 ($K_{\alpha 1}$)**	**0.66**
Pb	**2.34 ($M_{\alpha 1}$)**	**0.48**
Ti	4.49 ($K_{\alpha 1}$)	0.20

Figure S4 – EDX spectrum with energies of the lines used for analysis and resulting elemental composition of 497 sALD cycles PbS on TiO_2. The signal for Si is cut off to magnify the other signals.

The C 1s, N 1s, Ti 2p, O 1s and Na 1s XPS core level spectra of PbS (60 sALD cycles) deposited on TiO_2 are shown in **Figure S5**.

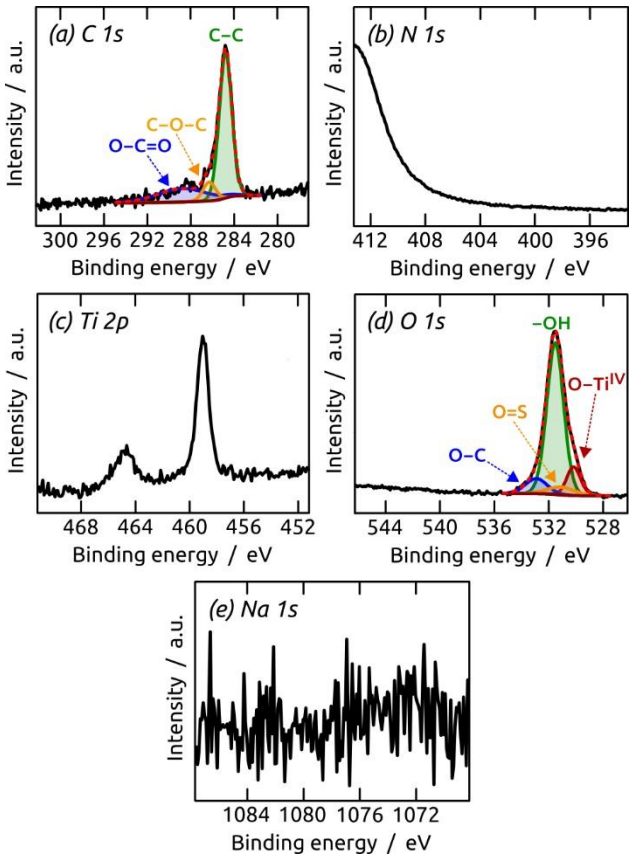

Figure S5 – XPS core level spectra of 60 sALD cycles PbS on TiO_2 (a) C 1s, (b) N 1s, (c) Ti 2p, (d) O 1s and (e) Na 1s.

The C 1s, N 1s, Ti 2p, O 1s and Na 1s XPS core level spectra of PbS (150 sALD cycles) deposited on TiO_2 are shown in **Figure S6**.

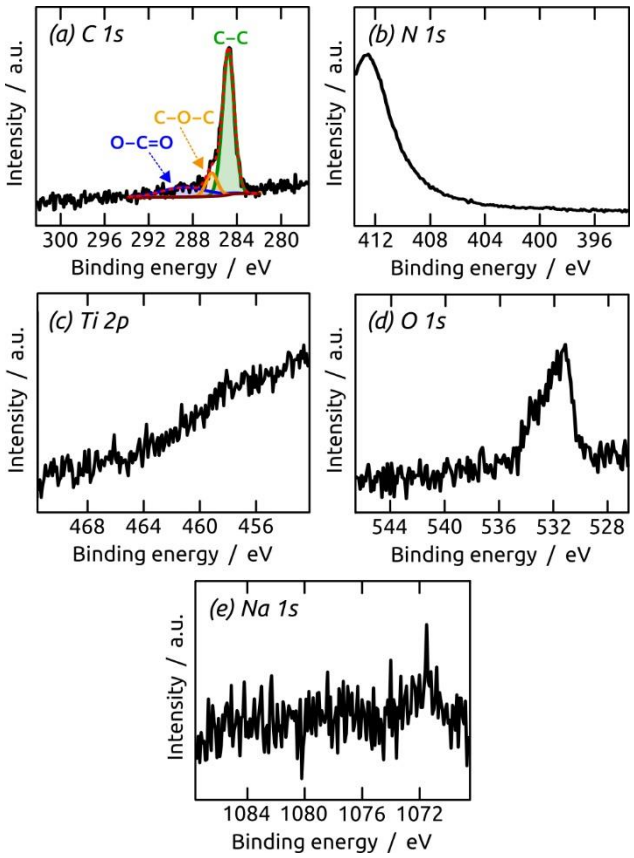

Figure S6 – XPS core level spectra of 150 sALD cycles PbS on TiO_2: (a) C 1s, (b) N 1s, (c) Ti 2p, (d) O 1s and (e) Na 1s.

Figure S7 shows (GI-) XRD diffractograms of a bare Si/SiO_2 wafer and 40 nm TiO_2 deposited *via* gALD on Si/SiO_2 wafer (annealed at 450 °C for 4 h). The diffraction signals can be attributed to the wafer (**Figure S7a**) and TiO_2 in the anatase phase[13,14] (**Figure S7b**).

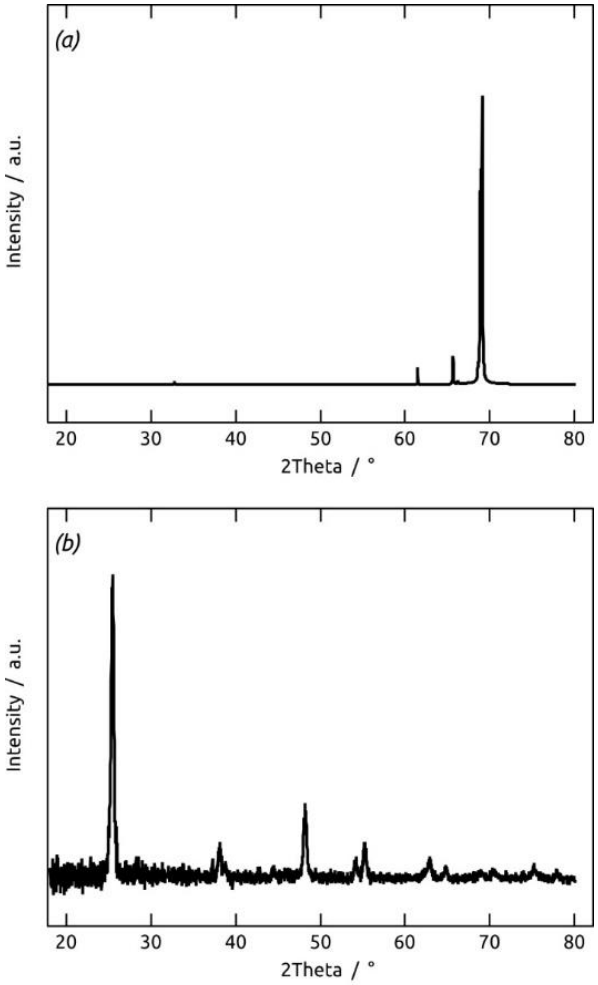

Figure S7 – (a) XRD diffractogram of bare Si/SiO_2 wafer, (b) GIXRD diffractogram of 40 nm anatase-TiO_2.

Characterization of the MAPI product

Figure S8 depicts cross-sectional SEM micrographs of PbS (250 and 497 cycles) deposited on TiO_2 (deposited *via* gALD on Si/SiO_2 wafers) and converted to MAPI. The thickness of the native SiO_2 layer is 200 nm, whereas the thickness of the TiO_2 layer is approximately 37 nm. The thickness of the PbS layers is approximately a) 28 nm (250 cycles) and c) 63 nm (497 cycles). The corresponding MAPI layers exhibit thicknesses of approximately b) 75 nm (converted from 250 cycles PbS) and d) 123 nm (converted from 497 cycles PbS).

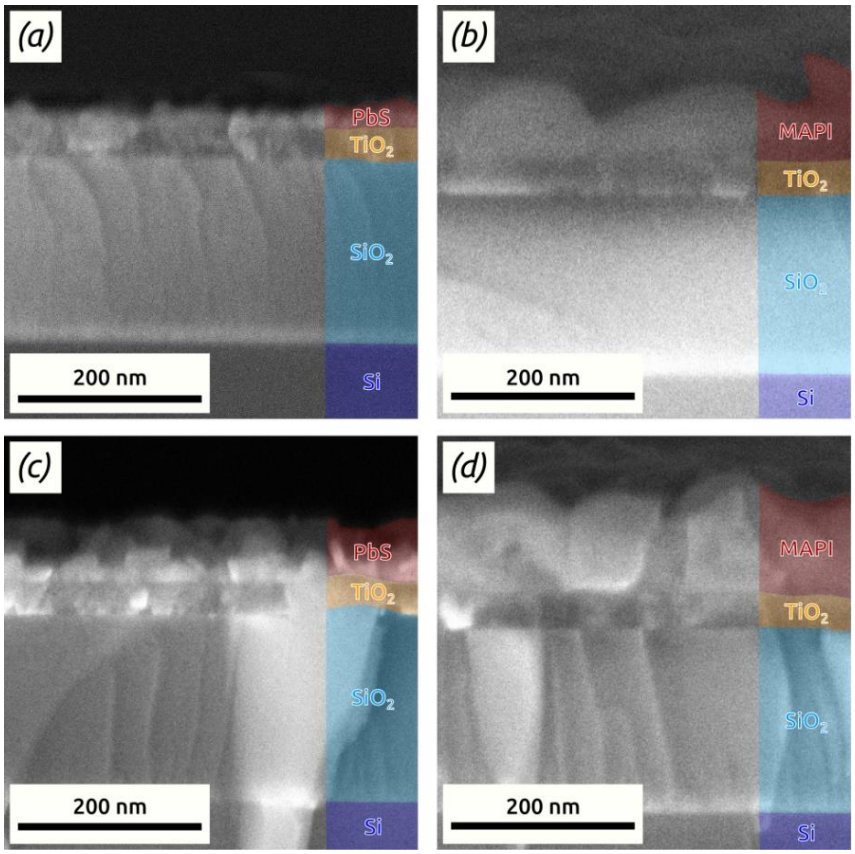

Figure S8 – Cross-sectional SEM micrographs of a) 250 cycles PbS, b) MAPI converted from 250 cycles PbS, c) 497 cycles PbS and d) MAPI converted from 497 cycles PbS on $TiO_2/SiO_2/Si$ substrates. The distinct layers are highlighted in colors: PbS or MAPI (red), TiO_2 (orange), SiO_2 (bright blue), Si (dark blue).

Figure S9 and **Figure S10** show the results of AFM measurements of PbS deposited on TiO_2 substrates (100, 250 and 497 cycles) and converted to MAPI**.** The thickness *d* of the PbS samples is a) 13 nm (100 cycles), b) 31 nm (250 cycles) and c) 65 nm (497 cycles) for PbS on TiO_2. The thicknesses of the corresponding MAPI samples on TiO_2 are d) 42 nm (converted from 100 cycles PbS), e) 70 nm (converted from 250 cycles PbS) and f) 129 nm (converted from 497 cycles PbS). The thickness values determined here are in good agreement with the values found in the cross-sectional SEM micrographs (**Figure S8**).

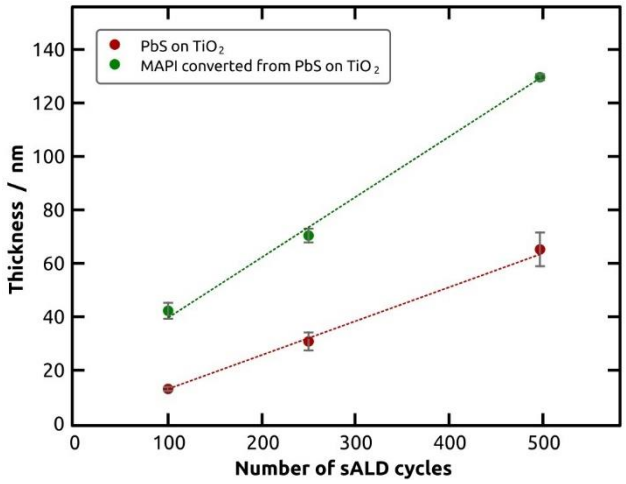

Figure S9 – Linear thickness increase with 100, 250 and 497 cycles of PbS sALD (red) and corresponding converted MAPI samples (green) on TiO_2.

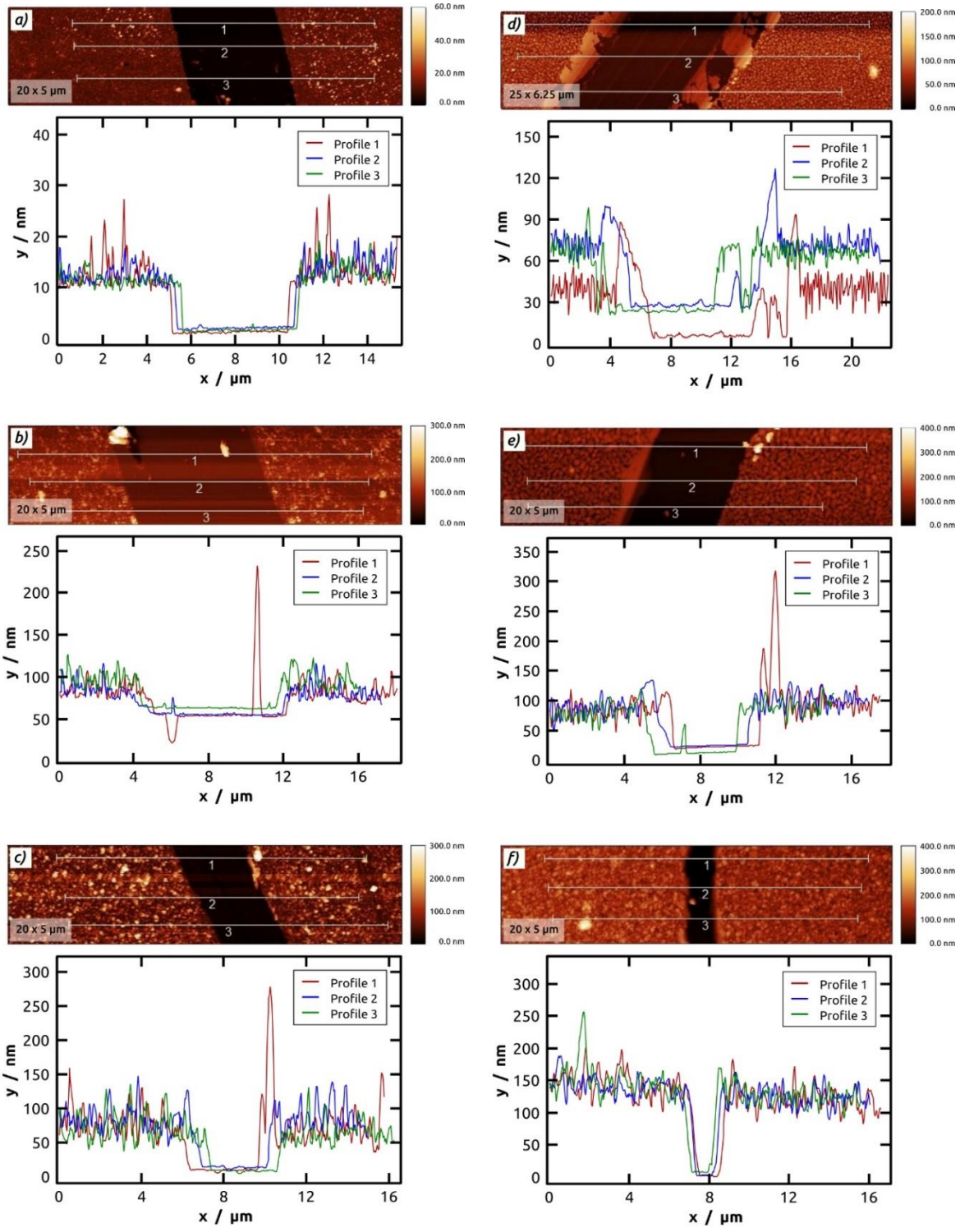

Figure S10 – AFM micrographs of a) 100 cycles PbS, b) 250 cycles PbS, c) 497 cycles PbS and MAPI converted from d) 100 cycles PbS, e) 250 cycles PbS and f) 497 cycles PbS on TiO_2.

Figure S11 depicts a cross sectional FE-SEM micrograph of PbS (80 sALD cycles) converted to MAPI in deep pores of 'anodic' aluminum oxide (AAO) membranes. The MAPI particles appear bright in the micrograph.

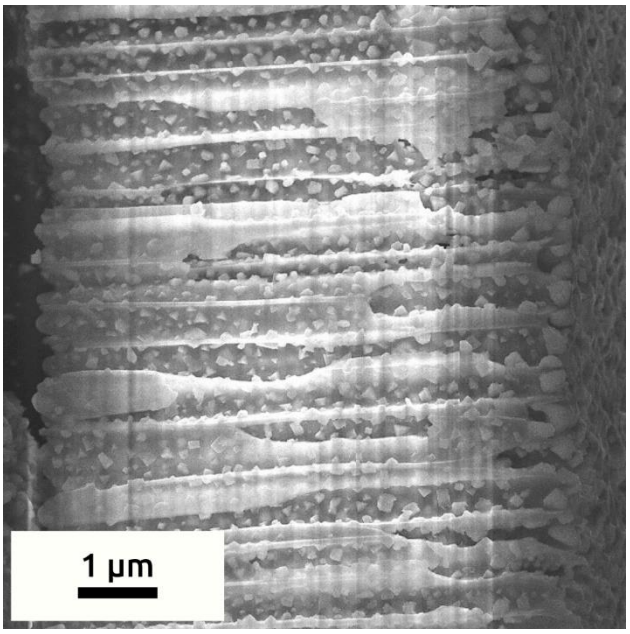

Figure S11 – Cross-sectional FE-SEM micrograph of an AAO membrane after conversion of 80 sALD cycles of PbS to MAPI.

Elemental analysis of a thick MAPI film (converted from PbS, 497 cycles on TiO_2) by EDX is shown in **Figure S12**. As expected, signals for C, N, Pb and I are detected in the EDX spectrum corresponding to MAPI. The signals for O, Si and Ti can be assigned to the substrate. The main contribution is Si at 1.74 eV ($K\alpha_1$) with 35.80 *at%* from the Si wafer. O at 0.52 eV ($K\alpha_1$) with 19.96 *at%* can be related to SiO_2 and TiO_2. The very small amount of Ti at 4.49 eV ($K\alpha_1$) with 0.20 *at%* indicates full coverage of the TiO_2. Signals for C and N are detected at 0.26 eV ($K\alpha_1$) and 0.39 eV ($K\alpha_1$), respectively. For Pb, signals are detected at 2.34 eV ($M\alpha_1$), 10.54 eV ($L\alpha_1$) and 12.62 eV ($L\alpha_1$). Signals at 3.94 eV ($L\alpha_1$) and at 4.21 eV ($L\alpha_1$) correspond to iodine.[12] Importantly, no sulfur was detected indicating full conversion from PbS to MAPI.

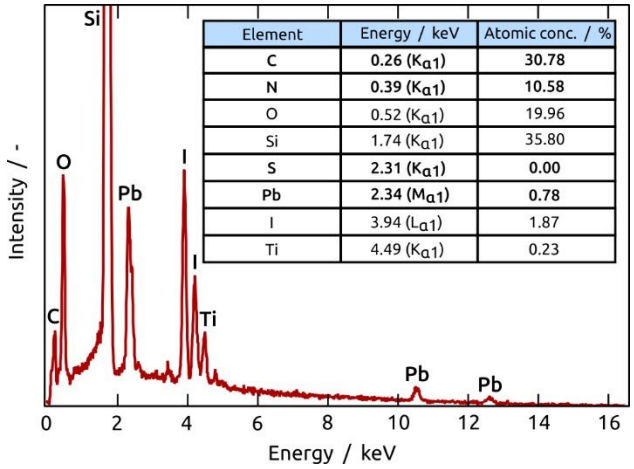

Element	Energy / keV	Atomic conc. / %
C	**0.26 ($K_{\alpha 1}$)**	**30.78**
N	**0.39 ($K_{\alpha 1}$)**	**10.58**
O	0.52 ($K_{\alpha 1}$)	19.96
Si	1.74 ($K_{\alpha 1}$)	35.80
S	**2.31 ($K_{\alpha 1}$)**	**0.00**
Pb	**2.34 ($M_{\alpha 1}$)**	**0.78**
I	3.94 ($L_{\alpha 1}$)	1.87
Ti	4.49 ($K_{\alpha 1}$)	0.23

Figure S12 – EDX spectrum with energies of the lines used for analysis and resulting elemental composition of MAPI (497 sALD cycles PbS on TiO_2 and converted to MAPI). The signal for Si is cut off to magnify the other signals.

The S 2p, C 1s, N 1s and Ti 2p XPS core level spectra of MAPI (converted from 497 sALD cycles of PbS on TiO_2) are shown in **Figure S13**. No sulfur species is detected in the S 2p scan. In the C 1s XPS scan, the main contribution results from C−C and C−H at 284.8 eV with a shoulder at 286.3 eV corresponding to carbon bound to oxygen and nitrogen, respectively. The C−H and C−N species can be assigned to the methylammonium ion in MAPI.[15] The small contribution at 288.8 eV for O−C=O is due to aerobic contamination.[16] The weak signal in the N 1s scan can be related to the methylammonium ion.[17] The Ti 2p scan shows oxidized Ti species from the TiO_2 substrate.[18]

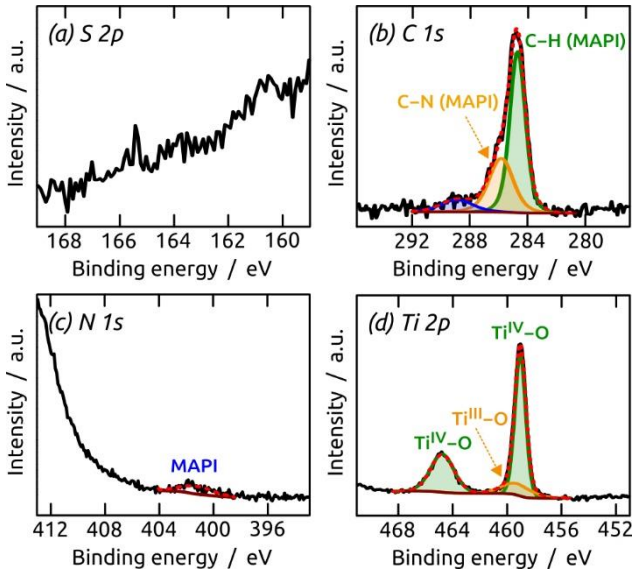

Figure S13 – XPS core level spectra of 497 sALD cycles of PbS converted to MAPI onTiO_2: a) S 2p, b) C 1s, c) N 1s and d) Ti 2p.

References

1 J. Choi, S. Song, M. T. Hörantner, H. J. Snaith, T. Park, *ACS Nano*, 2016, **10**, 6029—6036.

2 J.-P. Niemelä, G. Marin, M. Karppinen, Semicond. *Sci. and Technol*., 2017, **32**, 093005.

3 J. Aarik, A. Aidla, T. Uustare, M. Ritala, M. Leskelä, *Appl. Surf. Sci*., 2000, **161**, 385—395.

4 E. K. Seo, J. W. Lee, H. M. Sung-Suh, M. M. Sung, *Chem. Mater*., 2004, **16**, 1878—1883.

5 K. Aryal, Y. Erkaya, G. Rajan, T. Ashrafee, A. Rockett, R. W. Collins, S. Marsillac, presented in parts at IEEE 39th Photovoltaic Specialists Conference (PVSC), Tampa, FL, USA, June 2013.

6 N. Erkaya, D. Nminibapiel, K. Aryal, N. Hegde, G. Rajan, P. Boland, K. Zhang, H. Baumgart, S. Marsillac, *ECS Transactions*, 2013, **50**, 45—48.

7 S. Haschke, Y. Zhuo, S. Schlicht, M. K. S. Barr, R. Kloth, M. E. Dufond, L. Santinacci, J. Bachmann, *Adv. Mater. Interfaces*, 2019, **6**, 1801432.

8 Y. Wu, D. Döhler, M. Barr, E. Oks, M. Wolf, L. Santinacci, J. Bachmann, *Nano Lett*., 2015, **15**, 6379—6385.

9 J. Fichtner, Y. Wu, J. Hitzenberger, T. Drewello, J. Bachmann, *ECS J. Solid State Sci. Technol*., 2017, **6**, 171—175.

10 H. Abbas, R. Kottokkaran, B. Ganapathy, M. Samiee, L. Zhang, A. Kitahara, M. Noack, V. L. Dalal, *APL Materials*, 2015, **3**, 016105.

11 K. G. Stamplecoskie, J. S. Manser, P. V. Kamat, *Energy Environ. Sci*., 2015, **8**, 208—215.

12 Periodic Table of Elements and X-ray Energies. *Bruker* www.bruker.com/fileadmin/user_upload/8-PDF-Docs/X-rayDiffraction_ElementalAnalysis/HH-XRF/Misc/Periodic_Table_and_X-ray_Energies.pdf (accessed February 2019).

13 R. L. Parker, in *Zeitschrift für Kristallographie – Crystalline Materials*, Oldenbourg Wissenschaftsverlag GmbH, Munich, 59, 1924, Zur Kristallstruktur von Anatas und Rutil. (II. Teil. Die Anatasstruktur), 1—54.

14 P. Srinivasu, S. P. Singh, A. Islam, L. Han, *Advances in OptoElectronics*, 2011, 539382.

15 R. Wang C. Wu, Y. Hu, J. Li, P. Shen, Q. Wang, L. S. Liao, L. Liu, S. Duhm, *ACS Appl. Mater. Interfaces* 2017, **9**, 7859—7865.

16 XPS Interpretation of Carbon, *Thermo Fisher Scientific Inc.* https://xpssimplified.com/elements/carbon.php (accessed March 2019).

17 S. Olthof, K. Meerholz, *Sci. Rep.* 2017, **7**, 40267.

18 XPS Interpretation of Titanium, Thermo Fisher Scientific Inc. https://xpssimplified.com/elements/titanium.php (accessed March 2019).